Melting of the Vortex Lattice through Intermediate Hexatic Fluid in an *a*-MoGe Thin Film

Indranil Roy,[1] Surajit Dutta,[1] Aditya N. Roy Choudhury,[1] Somak Basistha,[1] Ilaria Maccari,[2] Soumyajit Mandal,[1] John Jesudasan,[1] Vivas Bagwe,[1] Claudio Castellani,[2] Lara Benfatto,[2] and Pratap Raychaudhuri[1,*]

[1]*Tata Institute of Fundamental Research, Homi Bhabha Road, Colaba, Mumbai 400005, India*

[2]*ISC-CNR and Department of Physics, Sapienza University of Rome, Piazzale Aldo Moro, 5, 00185 Rome, Italy*

(Received 16 May 2018; revised manuscript received 3 August 2018; published 30 January 2019)

The hexatic fluid refers to a phase in between a solid and a liquid that has short-range positional order but quasi-long-range orientational order. In the celebrated theory of Berezinskii, Kosterlitz, and Thouless and subsequently refined by Halperin, Nelson, and Young, it was predicted that a two-dimensional hexagonal solid can melt in two steps: first, through a transformation from a solid to a hexatic fluid, which retains quasi-long-range orientational order; and then from a hexatic fluid to an isotropic liquid. In this Letter, using a combination of real space imaging and transport measurements, we show that the two-dimensional vortex lattice in an *a-MoGe* thin film follows this sequence of melting as the magnetic field is increased. Identifying the signatures of various transitions on the bulk transport properties of the superconductor, we construct a vortex phase diagram for a two-dimensional superconductor.

DOI: 10.1103/PhysRevLett.122.047001

Ever since the seminal work [1] in which Berezinskii, Kosterlitz, and Thouless (BKT) predicted the possibility of a phase transition without breaking continuous symmetry in two-dimensional (2D) systems, a lot of effort has been devoted to explore its ramifications. 2D crystalline solids present an interesting situation. Melting of three-dimensional crystalline solids is understood through the "Lindemann criterion," where the solid melts through a first order phase transition when the lattice vibration amplitude exceeds a certain fraction of the lattice constant [2]. In contrast, for a 2D solid, the BKT theory extended subsequently by Halperin, Nelson, and Young (HNY) predicted that melting could also proceed through an alternate route [3–5] via two continuous phase transitions mediated via topological defects. At the first transition, thermally excited free dislocations proliferate in the lattice, creating an intermediate state between a crystalline solid and a liquid. At the second transition, dislocations dissociate into isolated disclinations producing an isotropic fluid. The intermediate state (called a hexatic fluid when the solid has hexagonal symmetry) has zero shear modulus and short-range positional order like in a liquid, but it retains the quasi-long-range orientational order of the parent solid. Over the years, there have been several attempts to test the BKTHNY theory in diverse 2D systems such as electrons over a liquid He surface [6], inert-gas monolayers adsorbed on graphite, vortices in superconducting thin films [7–10], and colloidal crystals [11–14]. Indeed, according to the various experimental conditions, one can either prove the occurrence of the melting transition at the expected value or the existence of an orientational order when the translational one is lost, but the simultaneous observation of the two features has so far been available only in the case of colloidal crystals [12–14].

In a clean conventional superconductor, the vortices arrange themselves into a hexagonal lattice, known as the Abrikosov vortex lattice (VL) [15,16]. In general, the vortices can meander along its length inside the superconductor, and therefore the VL is not strictly a 2D system. However, in thin films, the thickness of the sample can be orders of magnitude smaller than the characteristic bending length of the vortices [7]. In this limit, the vortices behave like point objects, and the VL behaves effectively like a 2D hexagonal solid. The progress in low temperature scanning tunneling spectroscopy (STS), which allows the imaging of the VL over a wide range of magnetic fields [17], has triggered efforts to directly observe the hexatic vortex fluid state. However, this simple scenario is complicated by the presence of additional ingredients. First, in crystalline superconducting films, the VL can get strongly coupled to the symmetry of the crystalline lattice [18–20], thereby influencing its orientational order. Second, crystalline defects and impurities create a random pinning landscape, which can trap vortices at specific locations. Although the first complicacy can be avoided in thin films of amorphous superconductors, some degree of random pinning is practically unavoidable.

From a theoretical standpoint, random pinning can easily destroy translational order, whereas its effect on orientational order is weaker. At low fields, it is now accepted that, in the presence of weak pinning, the VL is in a solidlike phase called Bragg glass [21–23], which has a long-range orientational order and a quasi-long-range positional order. However, at larger pinning density, the vortex state can become unstable to dislocations, even in the absence of thermal excitations [24–26], producing a hexatic glass. This disorder induced

hexatic glass differs from a hexatic fluid because of the fact that it has a nonzero shear modulus and the dislocations are frozen in space [27], unlike thermally generated dislocations in a hexatic fluid, which statistically appear at random locations. Although transport [8] or magnetic shielding measurements [7] can establish the melting of a Bragg glass fairly accurately, establishing the hexatic nature of a vortex state above the melting transition is not straightforward. On the other hand, real space imaging such as STS can identify a hexatic state from the quasi-long-range orientational order and the nature of topological defects [9,10,28–30], but because the dynamics of the vortices in the fluid phase can be extremely slow, it is not easy to distinguish between a hexatic glass and a hexatic fluid.

In this Letter, we adopt a strategy that combines magnetotransport and STS imaging to investigate the melting of the VL in a very weakly pinned amorphous MoGe (a-MoGe) thin film. The central result of this Letter is that, as the magnetic field is increased, the vortex state goes successively from a vortex solid to a hexatic fluid, and then to an isotropic liquid following the sequence expected from the BKTHNY theory.

In this study, we use a-MoGe thin films with thicknesses of $t \sim 20$ nm and $T_c \sim 7.05 \pm 0.05$ K, which are grown through pulsed laser deposition. The pinning strength, estimated from the depinning frequency of the vortex lattice at low fields (~35 kHz) is 6 orders of magnitude smaller than the corresponding values for Nb [31] or $YBa_2Cu_3O_7$ films [32,33]. The very weak pinning is further corroborated from the absence of any difference in the ac susceptibility measured in field cooled and zero field cooled states [34]. Further details are given in the Supplemental Material [35]. Because of different requirements of shape and size, two samples with the same T_c and a thickness variation of <10% were used for transport and STS measurements. For STS, postdeposition, the film was transferred in the scanning tunneling microscope using an ultrahigh vacuum suitcase without exposure to air.

We first investigate the transition from vortex solid to vortex fluid. Above a critical current, I_c, the Lorentz force on the vortices exceeds the pinning force and a flux flow regime is established. Here, the voltage is given by [43] $V = R_{\rm ff}(I - I_c)$, where $R_{\rm ff}$ is the flux flow resistance that is governed only by the viscous drag on individual vortices and independent of pinning [44]. Thus, the I-V characteristics for a vortex solid and a vortex fluid are similar for $I > I_c$. The distinctive features of a vortex solid and vortex fluid appear at $I \ll I_c$, where a small but finite voltage appears due to thermally activated flux flow (TAFF) over the pinning barrier, U, giving a TAFF resistance of $R_{\rm TAFF} = V/I = R_{\rm ff} \exp[-U(I)/kT]$, where k is the Boltzmann constant. For a vortex solid, $U(I)$ depends on current [22,45,46] as $U(I) = U_0 * (I_c/I)^{\alpha}$, such that $R_{\rm TAFF}$ (and V) exponentially goes to zero for $I \to 0$. In contrast, in a vortex fluid [47], $U(I)$, and hence

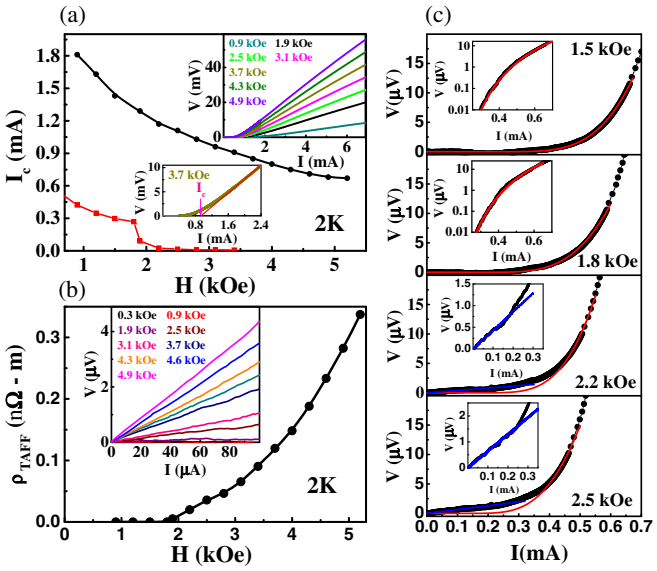

FIG. 1. (a) I_c vs H at 2 K (black circles); in the same plot is I_0, the current below which $V < 0.1$ μV (red square). Upper inset shows I-V curves at 2 K in different magnetic fields; some curves omitted for clarity. Lower inset illustrates linear fit (red line) to flux flow region from which I_c is determined. (b) $\rho_{\rm TAFF}$ as a function of magnetic field (black circles) and calculated from the low current region of I-V curves. Inset shows expanded view of I-V curves below 100 μA. (c) I-V curves for $I < I_c$ for four fields spanning vortex solid to vortex fluid transition. Red lines show fit to TAFF equation with $U = U_0 * (I_c/I)$ (U_0 is an adjustable parameter). Blue lines are linear fit to I-V curves below 100 μA. Insets of the upper two panels show same data in semilog scale, and insets of lower two panels show expanded view of linear fit.

$R_{\rm TAFF}$ is independent of current at low currents. In Fig. 1(a), we show I_c at 2 K in the magnetic field range of 0.9–5 kOe obtained by fitting the linear flux flow region of the I-V curves [Fig. 1(a), upper and lower insets]. To estimate $\rho_{\rm TAFF}$ ($I \to 0$), we investigate the I-V curve in the range of $I = 0 - 100$ μA ($\ll I_c$) [Fig. 1(b)]. Up to 1.9 kOe, the voltage is below our measurable limit; therefore, $\rho_{\rm TAFF} \approx 0$. Above 1.9 kOe, the I-V curves show a finite linear slope giving a finite $\rho_{\rm TAFF}$. To further confirm that this field corresponds to the vortex solid to vortex fluid transition, we investigate the functional form of the I-V curves for $I < I_c$ [Fig. 1(c)]. Below the transition (1.5 and 1.8 kOe), the I-V curves can be fitted very well with the form expected for a vortex solid with $\alpha = 1$. In contrast, above the transition (2.2 and 2.5 kOe), the I-V curves significantly deviate from the exponential dependence. Instead, at low currents, a linear slope appears below $I \approx 200$ μA as expected for a vortex fluid. The temperature dependence of $\rho_{\rm TAFF}$ above and below the melting field is consistent with this scenario [35].

To identify the nature of the vortex fluid, we use STS imaging. To obtain VL images, spatially resolved tunneling conductance [$G(V) = dI/dV$] was measured at different

fields using a Pt-Ir tip. The vortex core in a superconductor behaves like a normal metal in which both the gap and the coherence peak in the local density of states are suppressed. Consequently, when the bias voltage, V, is kept close to the superconducting coherence peak, each vortex manifests as a local minima [19,29,30] in $G(V)$. Figures 2(a)–2(f) show representative large area VL images at 2 K along with their 2D Fourier transforms (FTs). We obtain the precise positions of the vortices from the local minima in the conductance map and identify the topological defects by Delaunay triangulating the VL. At 1 kOe, we observe a hexagonal VL without any topological defects. Above 3 kOe, we observe free dislocations in the VL as expected for a vortex fluid. However, up to 70 kOe, the FT shows six spots, showing the existence of a sixfold orientational order. Above 70 kOe, the FT transforms into a ring corresponding to an isotropic vortex liquid. Because topological defects are free to move in a fluid, we expect the defects to appear at different locations when the VL is imaged at different times. In Fig. 3, we show three successive images of the VL captured over the same area, where the time to acquire each image is 1.5 h. In each image, dislocations appear at a different location and sometimes disappear from the field of view. Thus, our data are consistent with a hexatic vortex fluid below ~70 kOe and an isotropic vortex liquid at higher fields.

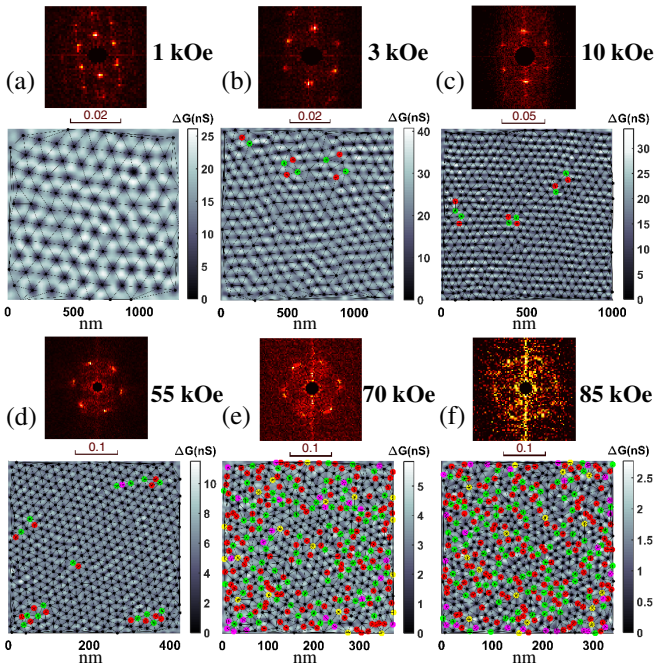

FIG. 2. (a)–(f) Representative vortex images at 2 K for different magnetic fields. Vortices (shown as black dots) appear as minima in conductance map recorded at a fixed dc bias: $V_b = 1.52$ mV. VL is Delaunay triangulated to find topological defects (denoted as red, green, magenta, and yellow dots) corresponding to five-, seven-, four-, and eightfold coordinations. Above each vortex image is the 2D FT of image; the scale bar is in nm^{-1}.

An important property of the hexatic fluid is that the motion of vortices should happen preferentially along the principal direction of the VL. To explore this, we follow the motion of the vortices on a finer scale by capturing a series of 12 successive images over the same area at 15 min intervals [Figs. 4(a)–4(i)]. Because no drive is applied here, the motion of the vortices is caused by stress relaxation of the VL. The stress in the VL could in principle be of two kinds: a residual global stress when the VL has not yet reached its true equilibrium, or local stress in the lattice caused by the appearance of short-lived dislocations. Although, in our sample, the global stress is unlikely to be an issue due to the very weak pinning nature of the film, as an added precaution, we apply several magnetic field pulses of 0.3 kOe before the data are taken. In the vortex solid phase (1 kOe; see Supplemental Material [35]), each vortex only undergoes a small wandering motion about its mean position. In the hexatic fluid (3 and 55 kOe), we observe that, although the motion of individual vortices is irregular and follows a jagged trajectory, over a longer timescale, all vortices within the field of view preferentially move along one of the three principal directions of the VL. This regularity of motion is disturbed in the vicinity of locations in which topological defects appear, where the movement becomes more random. On the other hand, at 85 kOe, the motion becomes completely random, as expected for an isotropic fluid.

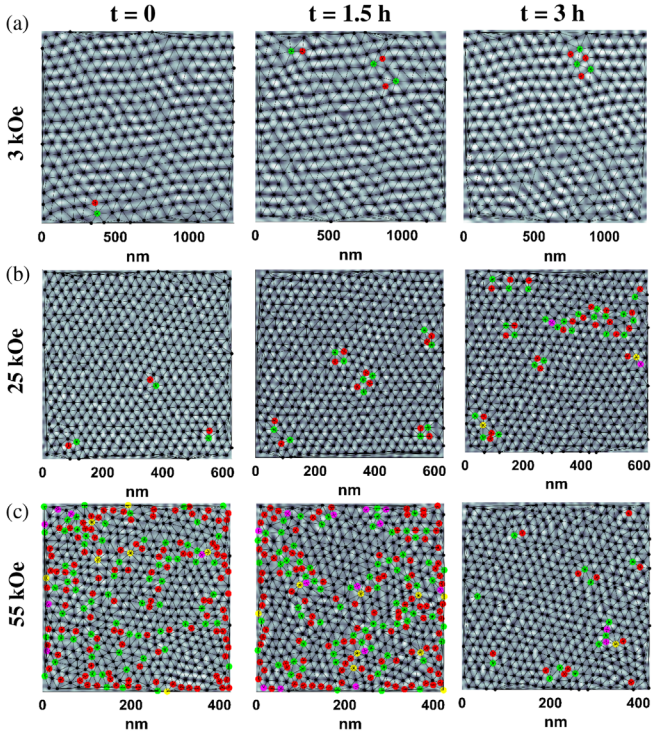

FIG. 3. (a)–(c) Three consecutive vortex images captured at same location at 2 K for 3, 25, and 55 kOe, respectively. Color scheme for vortices and defects is the same as in Fig. 2.

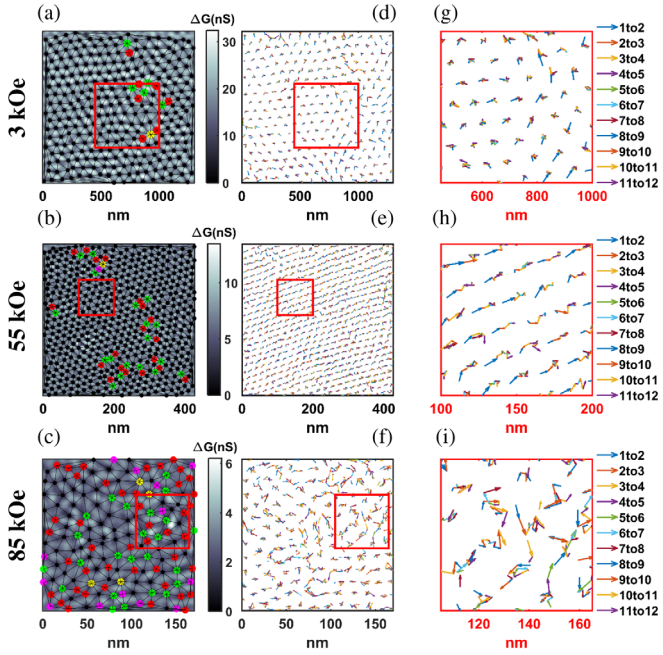

FIG. 4. (a)–(c) First image of 12 consecutive vortex images at 2 K for 3, 55, and 85 kOe, respectively. Color scheme for vortices and defects is the same as in Fig. 2. Figures 4(d)–4(f) are arrow maps for each field, in which each arrow gives displacement for every vortex through individual steps of 12 consecutive vortex images. Red boxes in arrow maps are enlarged in Figs. 4(g)–4(i).

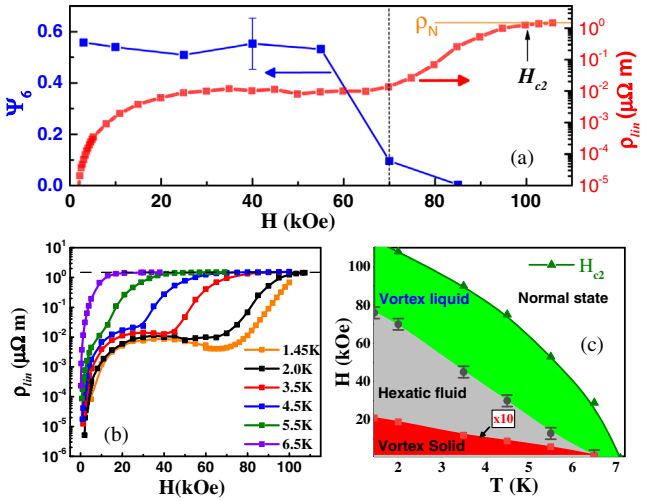

FIG. 5. (a) Variation of Ψ_6 and $\rho_{\rm lin}$ as function of magnetic field at 2 K. Representative error bar on Ψ_6 is shown on 40 kOe data point. Vertical dashed line demarcates hexatic fluid from vortex liquid. Horizontal orange line shows normal state resistivity, ρ_N. (b) $\rho_{\rm lin}$ vs H at different temperatures; horizontal dashed line denotes normal state resistivity. (c) Phase diagram showing vortex solid, hexatic fluid, and vortex liquid phase in H-T parameter space. Vortex solid and hexatic fluid phase boundary is multiplied by 10 on magnetic field axis for clarity.

To quantify the orientational order of the vortex state, we now compute the sixfold orientational order parameter [48], which is defined as $\Psi_6 = (1/N)\langle\sum_{k,l} e^{[6i(\phi_k-\phi_l)]}\rangle$; here, ϕ_k is the angle between a fixed direction in the plane of the VL and the kth bond, and the sum runs over all the bonds in the VL. $\Psi_6 = 1$ for a perfect hexagonal lattice. To improve the statistics, we average over the series of 12 images. In Fig. 5(a), we plot the magnetic field variation of Ψ_6 at 2 K. Ψ_6 remains finite up to 55 kOe and abruptly drops to a small value above 70 kOe, signaling the transition from a hexatic fluid to a vortex liquid [49]. On the same plot, we show $\rho_{\rm lin}$ extracted from the linear slope of the I-V curve below 100 μA. Above 70 kOe, $\rho_{\rm lin}$ increases rapidly, reflecting the increased mobility of the vortices as the system enters the isotropic vortex liquid state and then saturates to the normal state value of $\rho_N \sim 1.51\ \mu\Omega\,\mathrm{m}$. Consequently, we define the transition from the hexatic vortex fluid to isotropic liquid from the magnetic field, where $\rho_{\rm lin}$ starts to increase; and we define H_{c2} as the field where $\rho_{\rm lin} \approx 0.95\rho_N$, with the error bar given by the magnetic field interval at which the data are taken. We note that, above 80 kOe, I_c becomes small and we cannot unambiguously identify $\rho_{\rm lin}$ with $\rho_{\rm TAFF}$. At low temperatures, we also observe a shallow minimum in $\rho_{\rm lin}$, which is reminiscent of the more pronounced "peak effect" observed at the order-disorder transition in thicker samples [50]. This can be understood within the collective weak pinning scenario [51], in which the orientational stiffness modulus (Frank constant) [13] of the hexatic vortex fluid plays the role of the shear modulus and the length scale analogous to the Larkin length, R_c, is given by the average length scale of dislocation free regions governed by dislocation density [35].

We can now use the $\rho_{\rm lin}$-H variation at different temperatures [Fig. 5(b)] to construct the phase diagram in the H-T parameter space [Fig. 5(c)]. It is interesting to note that both the solid-hexatic fluid and the hexatic fluid-vortex liquid phase boundaries keep increasing in field down to the lowest temperature, as expected for the thermal melting transition [8], instead of flattening out at low temperatures, as often observed when the order-disorder transition is driven by disorder [22,52]. Further investigation is needed to determine to what extent this phase diagram could be generic, for example, in thin crystalline superconductors (such as monolayer [53] $NbSe_2$) or for the quasi-2D VL in layered high-T_c cuprates [54]. Finally, we would also like to note that, although we have used the magnetic field (or, alternatively, the density of vortices) as the tuning parameter, one would also expect to observe the two-step melting as a function of temperature. However, it might be more difficult to observe the transition as a function of temperature in imaging experiments because the contrast in STS images becomes poor at elevated temperatures.

In summary, we have shown a clear demonstration of the BKTHNY type two-step melting of the 2D vortex lattice in a very weakly disordered a-MoGe thin film. We believe that the simplicity of the system combined with the ability to investigate the static and dynamic response of the VL using different probes, such as high frequency conductivity

and precision magnetometry, will pave the way to a more detailed understanding of defect driven phase transitions.

P. R. would like to thank Nandini Trivedi and L. B. would like to thank Thierry Giamarchi and Dragana Popovic for valuable discussions. We would like to thank Arumugam Thamizhavel for his help in preparing the MoGe target. The work was supported by the Department of Atomic Energy, Govt. of India; the Department of Science and Technology, Govt. of India (Grant No. EMR/2015/000083); and the India–Italy joint project [Grants No. INT/Italy/P-21/2016 (SP) and No. MAECI SUPERTOP-PGRO4879].

I. R., S. D., and S. M. performed the scanning tunneling spectroscopy measurements and analyzed the data. S. D., A. N. R. C., and S. B. performed the transport and penetration depth measurements and analyzed the data. A. N. R. C., J. J., and V. B. synthesized the sample and performed basic characterization. The physical picture was refined through discussions with I. M., C. C., and L. B. P. R. conceived the problem, supervised the project, and wrote the Letter. All authors read the manuscript and commented on the Letter.

*pratap@tifr.res.in

[1] J. M. Kosterlitz and D. J. Thouless, Early work on defect driven phase transitions, in *40 Years of Berezinskii-Kosterlitz-Thouless Theory*, edited by J. V. Jose (World Scientific, Singapore, 2013), ISBN: 978-9814417631.

[2] F. A. Lindemann, The calculation of molecular vibration frequencies, Phys. Z. **11**, 609 (1910).

[3] B. I. Halperin and D. R. Nelson, Theory of Two-Dimensional Melting, Phys. Rev. Lett. **41**, 121 (1978); **41**, 519 (1978).

[4] A. P. Young, Melting and the vector Coulomb gas in two dimensions, Phys. Rev. B **19**, 1855 (1979).

[5] V. N. Ryzhov, E. E. Tareyeva, Y. D. Fomin, and E. N. Tsiok, Berezinskii–Kosterlitz–Thouless transition and two-dimensional melting, Phys. Usp. **60**, 857 (2017).

[6] W. F. Brinkman, D. S. Fisher, and D. E. Moncton, Melting of two-dimensional solids, Science **217**, 693 (1982).

[7] A. Yazdani, C. M. Howald, W. R. White, M. R. Beasley, and A. Kapitulnik, Competition between pinning and melting in the two-dimensional vortex lattice, Phys. Rev. B **50**, R16117 (1994).

[8] P. Berghuis, A. L. F. van der Slot, and P. H. Kes, Dislocation-Mediated Vortex-Lattice Melting in Thin Films of a-Nb_3Ge, Phys. Rev. Lett. **65**, 2583 (1990).

[9] I. Guillamón, H. Suderow, A. Fernández-Pacheco, J. Sesé, R. Córdoba, J. M. De Teresa, M. R. Ibarra, and S. Vieira, Direct observation of melting in a two-dimensional superconducting vortex lattice, Nat. Phys. **5**, 651 (2009).

[10] I. Guillamón, R. Córdoba, J. Sesé, J. M. De Teresa, M. R. Ibarra, S. Vieira, and H. Suderow, Enhancement of long-range correlations in a 2D vortex lattice by an incommensurate 1D disorder potential, Nat. Phys. **10**, 851 (2014).

[11] R. E. Kusner, J. A. Mann, J. Kerins, and A. J. Dahm, Two-Stage Melting of a Two-Dimensional Collodial Lattice with Dipole Interactions, Phys. Rev. Lett. **73**, 3113 (1994).

[12] K. Zahn, R. Lenke, and G. Maret, Two-Stage Melting of Paramagnetic Colloidal Crystals in Two Dimensions, Phys. Rev. Lett. **82**, 2721 (1999).

[13] P. Keim, G. Maret, and H. H. von Grünberg, Frank's constant in the hexatic phase, Phys. Rev. E **75**, 031402 (2007).

[14] S. Deutschlander, T. Horn, H. Lowen, G. Maret, and P. Keim, Two-Dimensional Melting under Quenched Disorder, Phys. Rev. Lett. **111**, 098301 (2013).

[15] A. A. Abrikosov, The magnetic properties of superconducting alloys, J. Phys. Chem. Solids **2**, 199 (1957).

[16] L. P. Lévy, Vortices in type II superconductors, in *Magnetism and Superconductivity: Texts and Monographs in Physics* (Springer, Berlin, Heidelberg, 2000), ISBN: 978-3642085956.

[17] H. Suderow, I. Guillamón, J. G. Rodrigo, and S. Vieira, Imaging superconducting vortex cores and lattices with a scanning tunneling microscope, Supercond. Sci. Technol. **27**, 063001 (2014).

[18] J. Toner, Orientational Order in Disordered Superconductors, Phys. Rev. Lett. **66**, 2523 (1991).

[19] S. C. Ganguli, H. Singh, R. Ganguly, V. Bagwe, A. Thamizhavel, and P. Raychaudhuri, Orientational coupling between the vortex lattice and the crystalline lattice in a weakly pinned $Co_{0.0075}NbSe_2$ single crystal, J. Phys. Condens. Matter **28**, 165701 (2016).

[20] V. G. Kogan, M. Bullock, B. Harmon, P. Miranovic, Lj. Dobrosavljevic-Grujic, P. L. Gammel, and D. J. Bishop, Vortex lattice transitions in borocarbides, Phys. Rev. B **55**, R8693 (1997).

[21] T. Giamarchi and P. Le Doussal, Elastic theory of flux lattices in the presence of weak disorder, Phys. Rev. B **52**, 1242 (1995).

[22] T. Giamarchi and P. Le Doussal, Phase diagrams of flux lattices with disorder, Phys. Rev. B **55**, 6577 (1997).

[23] T. Giamarchi, Disordered elastic media, in *Encyclopaedia of Complexity and Systems Science*, edited by R. Meyers (Springer, New York, 2009), ISBN: 978-0387758886.

[24] E. M. Chudnovsky, Structure of a solid film on an imperfect surface, Phys. Rev. B **33**, 245 (1986); Hexatic vortex glass in disordered superconductors, Phys. Rev. B **40**, 11355(R) (1989); Orientational, and positional order in flux lattices of type-II superconductors, Phys. Rev. B **43**, 7831 (1991).

[25] M.-C. Cha and H. A. Fertig, Disorder-Induced Phase Transitions in Two-Dimensional Crystals, Phys. Rev. Lett. **74**, 4867 (1995).

[26] S. Herrera-Velarde and H. H. von Grunberg, Disorder-induced vs temperature-induced melting of two-dimensional colloidal crystals, Soft Matter **5**, 391 (2009).

[27] J. P. Rodriguez, Macroscopic phase coherence of defective vortex lattices in two dimensions, Phys. Rev. B **72**, 214503 (2005).

[28] M. Zehetmayer, How the vortex lattice of a superconductor becomes disordered: A study by scanning tunneling spectroscopy, Sci. Rep. **5**, 9244 (2015).

[29] S. C. Ganguli, H. Singh, G. Saraswat, R. Ganguly, V. Bagwe, P. Shirage, A. Thamizhavel, and P. Raychaudhuri,

Disordering of the vortex lattice through successive destruction of positional and orientational order in a weakly pinned $Co_{0.0075}NbSe_2$ single crystal, Sci. Rep. **5**, 10613 (2015).

[30] S. C. Ganguli, H. Singh, I. Roy, V. Bagwe, D. Bala, A. Thamizhavel, and P. Raychaudhuri, Disorder-induced two-step melting of vortex matter in Co-intercalated $NbSe_2$ single crystals, Phys. Rev. B **93**, 144503 (2016).

[31] D. Janjušević, M. S. Grbić, M. Požek, A. Dulčić, D. Paar, B. Nebendahl, and T. Wagner, Microwave response of thin niobium films under perpendicular static magnetic fields, Phys. Rev. B **74**, 104501 (2006).

[32] A. A. Pesetski and T. R. Lemberger, Experimental study of the inductance of pinned vortices in superconducting $YBa_2Cu_3O_{7-\delta}$ films, Phys. Rev. B **62**, 11826 (2000).

[33] M. Golosovsky, M. Tsindlekht, and D. Davidov, High-frequency vortex dynamics in $YBa_2Cu_3O_7$, Supercond. Sci. Technol. **9**, 1 (1996).

[34] M. Marziali Bermudez, E. R. Louden, M. R. Eskildsen, C. D. Dewhurst, V. Bekeris, and G. Pasquini, Metastability and hysteretic vortex pinning near the order-disorder transition in $NbSe_2$: Interplay between plastic and elastic energy barriers, Phys. Rev. B **95**, 104505 (2017).

[35] See Supplemental Material at http://link.aps.org/supplemental/10.1103/PhysRevLett.122.047001 for details on sample growth and characterization, spatial variation of the orientational order parameter $G_6(r)$, temperature dependence of ρ_{TAFF}, real space visualization of vortex creep, and the origin of the "peak effect," which includes Refs. [36–42].

[36] S. J. Turneaure, E. R. Ulm, and T. R. Lemberger, Numerical modeling of a two-coil apparatus for measuring the magnetic penetration depth in superconducting films and arrays, J. Appl. Phys. **79**, 4221 (1996).

[37] A. Kamlapure, M. Mondal, M. Chand, A. Mishra, J. Jesudasan, V. Bagwe, L. Benfatto, V. Tripathi, and P. Raychaudhuri, Measurement of magnetic penetration depth and superconducting energy gap in very thin epitaxial NbN films, Appl. Phys. Lett. **96**, 072509 (2010).

[38] I. Roy, P. Chauhan, H. Singh, S. Kumar, J. Jesudasan, P. Parab, R. Sensarma, S. Bose, and P. Raychaudhuri, Dynamic transition from Mott-like to metal-like state of the vortex lattice in a superconducting film with a periodic array of holes, Phys. Rev. B **95**, 054513 (2017).

[39] A. Kamlapure, G. Saraswat, S. C. Ganguli, V. Bagwe, P. Raychaudhuri, and S. P. Pai, A 350 mK, 9 T scanning tunnelling microscope for the study of superconducting thin films on insulating substrates and single crystals, Rev. Sci. Instrum. **84**, 123905 (2013).

[40] M. Tinkham, *Introduction to Superconductivity, Second Edition* (McGraw-Hill, New York, 1996), ISBN: 978-0486435039.

[41] R. C. Dynes, V. Narayanamurti, and J. P. Garno, Direct Measurement of Quasiparticle-Lifetime Broadening in a Strong-Coupled Superconductor, Phys. Rev. Lett. **41**, 1509 (1978).

[42] E. H. Brandt, Penetration of Magnetic ac Fields into Type-II Superconductor, Phys. Rev. Lett. **67**, 2219 (1991).

[43] T. P. Orlando and K. A. Delin, *Foundations of Applied Superconductivity* (Addison-Wesley, Reading, MA, 1991), ISBN: 978-0201183238.

[44] J. B. Ketterson and S. N. Song, *Superconductivity* (Cambridge University Press, Cambridge, 1999), ISBN: 978-0521565622.

[45] M. V. Feigel'man, V. B. Geshkenbein, A. I. Larkin, and V. M. Vinokur, Theory of Collective Flux Creep, Phys. Rev. Lett. **63**, 2303 (1989).

[46] D. S. Fisher, M. P. A. Fisher, and D. A. Huse, Thermal fluctuations, quenched disorder, phase transitions, and transport in type-II superconductors, Phys. Rev. B **43**, 130 (1991).

[47] V. M. Vinokur, M. V. Feigel'man, V. B. Geshkenbein, and A. I. Larkin, Resistivity of High-T_c Superconductors in a Vortex-Liquid State, Phys. Rev. Lett. **65**, 259 (1990).

[48] S. A. Hattel and J. M. Wheatley, Flux-lattice melting and depinning in the weakly frustrated two-dimensional XY model, Phys. Rev. B **51**, 11951 (1995).

[49] The small but finite value of Ψ_6 observed at 70 kOe results from the large short-range orientation correlation length close to the hexatic fluid-vortex liquid boundary; see Ref. [35].

[50] R. Wordenweber, P. H. Kes, and C. C. Tsuei, Peak and history effects in two-dimensional collective flux pinning, Phys. Rev. B **33**, 3172 (1986).

[51] A. I. Larkin and Y. N. Ovchinnikov, Pinning in type II superconductors, J. Low Temp. Phys. **34**, 409 (1979).

[52] B. Khaykovich, E. Zeldov, D. Majer, T. W. Li, P. H. Kes, and M. Konczykowski, Vortex-Lattice Phase Transitions in $Bi_2Sr_2CaCu_2O_8$ Crystals with Different Oxygen Stoichiometry, Phys. Rev. Lett. **76**, 2555 (1996).

[53] H. Wang *et al.*, High-quality monolayer superconductor $NbSe_2$ grown by chemical vapour deposition, Nat. Commun. **8**, 394 (2017).

[54] Z. Shi, P. G. Baity, T. Sasagawa, and D. Popović, Unveiling the phase diagram of a striped cuprate at high magnetic fields: Hidden order of Cooper pairs, arXiv:1801.06903v1.